JACS Au
AN OPEN ACCESS JOURNAL OF THE AMERICAN CHEMICAL SOCIETY

pubs.acs.org/jacsau

Article

Boosting Thermal Stability of Volatile Os Catalysts by Downsizing to Atomically Dispersed Species

Jae Hyung Kim,[‖] Sinmyung Yoon,[‖] Du San Baek,[‖] Jihun Kim, Jinjong Kim, Kwangjin An,* and Sang Hoon Joo*

Cite This: *JACS Au* 2022, 2, 1811−1817

Read Online

ACCESS | Metrics & More | Article Recommendations | Supporting Information

ABSTRACT: Os-based catalysts present remarkable catalytic activity; however, their use has been limited by the undesirable side reactions that generate highly toxic and volatile OsO_4 even at room temperature. Herein, we demonstrate that the thermal stability of Os-based catalysts can be dramatically improved by downsizing Os nanoparticles (NPs) into atomically dispersed species. We observed that Os NPs were converted into OsO_4 after calcination at 250 °C followed by sublimation, whereas single Os sites retained their structure after calcination. Temperature-programmed oxidation analysis confirmed that Os NPs started to undergo oxidation at 130 °C, whereas atomically dispersed Os preserved its state up to 300 °C. The CO oxidation activity of the atomically dispersed Os catalyst at 400 °C (100% conversion) was stably preserved over 30 h. By contrast, the activity of Os NP catalyst declined drastically. This study highlights the unique catalytic behavior of atomically dispersed catalysts, which is distinct from that of NP-based catalysts.

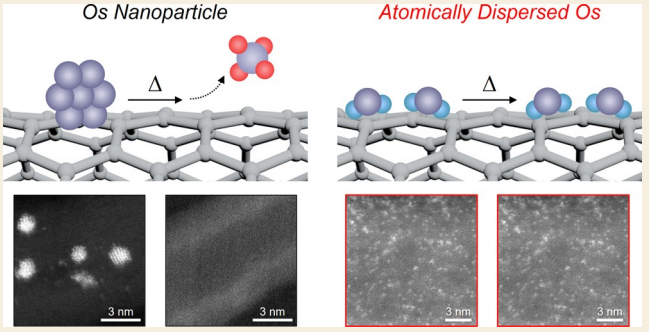

KEYWORDS: *osmium catalysts, osmium tetroxide, atomically dispersed catalysts, thermal stability, CO oxidation*

INTRODUCTION

Os-based catalysts are an important family of catalytic materials with broad utility in numerous catalytic processes, including asymmetric dihydroxylation,[1,2] hydrogenation,[3,4] and dehydrogenation reactions.[5] Despite the appealing catalytic performance of Os, its high toxicity has limited its catalytic applications.[6] Os can react with O_2 even at ambient temperatures, generating volatile osmium tetroxide (OsO_4). The occupational safety and health administration permissible exposure limit of OsO_4 is 0.002 mg m^{-3}, which is significantly lower than that of Hg vapor (0.1 mg m^{-3}).[7] Furthermore, the high volatility of OsO_4 hinders the reuse of Os catalysts, impeding their commercial development. To mitigate the toxicity and volatility shortcomings, Os-based complexes have been immobilized onto organic or inorganic supports, such as polymers, silica (SiO_2), fullerenes, and metal oxides.[8−19] Immobilization improved catalyst stability and recyclability; however, Os leaching has still occurred because of the weak interactions between the Os species and the supports.[17,19]

Recently, with the emergence of atomically dispersed catalysts, new, interesting findings have been uncovered in the field of catalysis.[20−27] Atomically dispersed catalysts have demonstrated unprecedented intrinsic activities or unique selectivities in diverse reactions,[28−34] which have not been displayed by conventional nanoparticle (NP)-based catalysts.

In this study, we discover that highly volatile Os can be transformed into a thermally stable catalyst by downsizing Os into atomically dispersed species. The atomically dispersed Os catalyst exhibited remarkable stability against oxidation into OsO_4. Single atomic Os species anchored on heteroatom-doped carbon supports were stably preserved after calcination at 250 °C. In contrast, Os NPs were converted into OsO_4 during calcination, which underwent subsequent sublimation. Temperature-programmed oxidation (TPO) analysis revealed that Os NPs started to undergo oxidation at ∼130 °C, whereas atomically dispersed Os catalysts were stable against oxidation up to 300 °C. By virtue of its excellent thermal stability, the atomically dispersed Os catalyst exhibited stable 100% CO conversion over 30 h during the CO oxidation reaction. In contrast, the CO conversion of the Os NP catalyst decreased significantly from 100% to only ∼15% after 30 h due to Os NP conversion into OsO_4 followed by sublimation. These findings suggest a possibility of thermally stable Os catalysts that have

Received: February 13, 2022
Revised: May 11, 2022
Accepted: May 13, 2022
Published: May 26, 2022

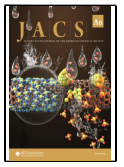

https://doi.org/10.1021/jacsau.2c00090
JACS Au 2022, 2, 1811−1817

been hard to realize and demonstrate the remarkable potential of atomically dispersed catalysts.

RESULTS AND DISCUSSION

Synthesis and Characterization of Os-Based Catalysts

This study was motivated by an accidental observation. In a previous study, we prepared an Os NP-based catalyst and an atomically dispersed Os catalyst.[35] After several months, we observed that the lid of a vial containing the Os NP catalyst was stained dark because OsO_4 was generated at room temperature. In contrast, the lid of the vial containing the atomically dispersed Os catalyst was not stained (Figure S1). From this observation, we hypothesized that unlike Os NPs, atomically dispersed Os can serve as a thermally stable catalyst.

The Os NP-based and atomically dispersed Os catalysts were synthesized according to the methods described in a previous study with some modifications.[35] The Os NP catalyst was prepared via the wet impregnation of dihydrogen hexachloroosmate(IV) hydrate ($H_2OsCl_6{\cdot}xH_2O$) on an acid-treated carbon nanotube (CNT) support, followed by H_2 thermal activation. The product is denoted as Os NP/CNT. To prepare the atomically dispersed Os catalyst, 1-butyl-3-methylimidazolium bis-(trifluoromethylsulfonyl)imide ionic liquid (IL) was coated onto CNTs to provide sufficient heteroatom anchoring sites for the Os precursor. $H_2OsCl_6{\cdot}xH_2O$ was impregnated onto the obtained CNT_IL support via wet impregnation, and the resulting sample was coated with a SiO_2 protective layer to prevent Os agglomeration during thermal activation at 500 °C under a N_2 atmosphere.[36] After thermal activation, the SiO_2 protective layer was selectively removed via HF etching. The obtained catalyst is denoted as Os_1/CNT_IL (see details in the Materials and Methods section).

The high-angle annular dark-field scanning transmission electron microscopy (HAADF-STEM) images of the Os NP/CNT and Os_1/CNT_IL catalysts (Figure 1a,b, respectively) revealed the presence of heterogeneously distributed Os NPs with an average size of ∼1.1 nm in the Os NP/CNT (Figure S2a) and atomically dispersed Os species on the support in the Os_1/CNT_IL (Figure S2b). The extended X-ray absorption fine structure (EXAFS) analyses (Figures S3 and S4 and Table S1) corroborated the HAADF-STEM results. The Os L_3-edge k^3-weighted EXAFS spectrum of the Os NP/CNT exhibited two scattering peaks: an Os−Os scattering peak at 2.5 Å, which is ascribed to the metallic Os NPs, and an Os−C(O) scattering peak at 1.8 Å, which is attributed to the bonds between Os and the support (Figure S3). The EXAFS spectrum of Os_1/CNT_IL showed only an Os−N(C,O) scattering peak at 1.8 Å, demonstrating the absence of the Os NP from Os_1/CNT_IL (Figure S4). The deconvoluted N 1s X-ray photoelectron spectroscopy (XPS) spectra of CNT_IL and Os_1/CNT_IL showed the generation of the Os−N bond after embedding Os atoms on CNT_IL (Figure S5), which indicates that the single Os atoms are mostly bound onto N in Os_1/CNT_IL. X-ray absorption near edge structure (XANES) analyses also provided information on the catalyst structures (Figure S6). The Os L_3-edge XANES spectrum of the Os NP/CNT displayed a whiteline peak and a peak in the post-edge region (peaks *A* and *B*, respectively), which are attributed to metallic Os.[37,38] In contrast, peak *B* was absent in the Os L_3-edge XANES spectrum of Os_1/CNT_IL. The intensity of the whiteline peak in the XANES spectrum of Os_1/CNT_IL was higher than that of Os NP/CNT. Moreover, the blue-shifted edge of Os_1/CNT_IL was compared with that of Os NP/CNT, indicating the ionic character of the atomically dispersed catalyst.[20]

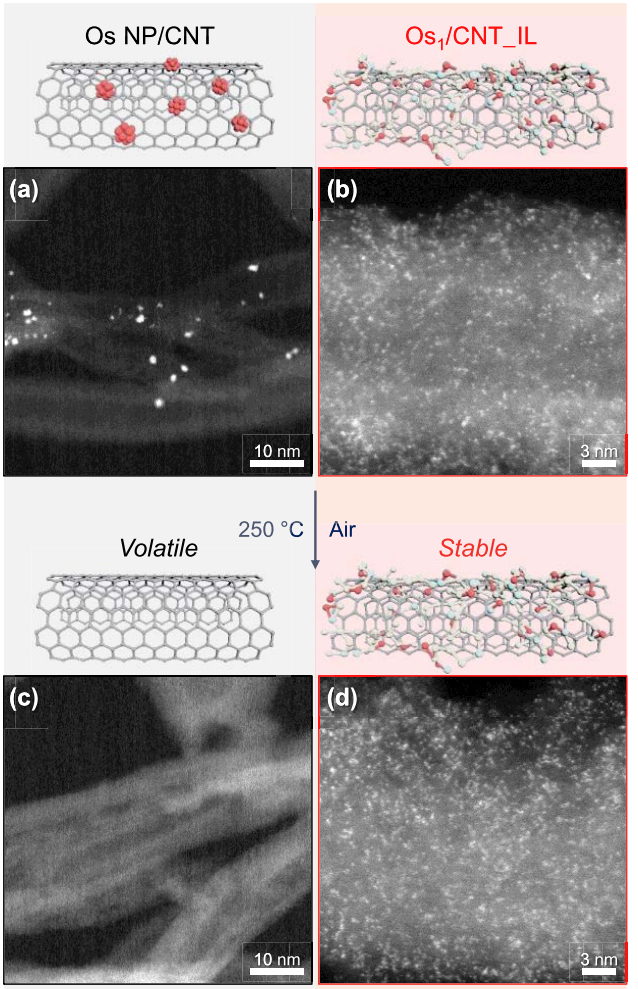

Figure 1. Schematic illustrations and HAADF-STEM images of the (a) as-prepared and (c) calcined Os NP/CNT at 250 °C and (b) as-prepared and (d) calcined Os_1/CNT_IL at 250 °C.

Difference in Thermal Stability between Os NPs and Atomically Dispersed Os

We investigated the thermal stability of both Os catalysts against the reaction with O_2 to form OsO_4. To accelerate the reaction, a stability test was performed at 250 °C for 10 h under static air conditions. Catalyst stability was readily evaluated using their HAADF-STEM images. After calcination, the Os NPs in Os NP/CNT disappeared because they were converted into OsO_4, which subsequently sublimated (Figures 1a,c and S7), whereas the atomically dispersed Os sites of Os_1/CNT_IL retained their isolated structure (Figures 1b,d and S8). We also analyzed the volatility of the Os catalysts by measuring their Os contents before and after calcination using inductively coupled plasma-optical emission spectroscopy (ICP-OES). The Os contents of the as-prepared Os NP/CNT and Os_1/CNT_IL catalysts were 2.66 and 1.54 wt %, respectively (Table S2). After calcination, a negligible residual amount of Os (0.01 wt %) was present in Os NP/CNT, whereas the Os content of Os_1/CNT_IL was maintained (1.58 wt %; Table S2). These results demonstrated the remarkable

https://doi.org/10.1021/jacsau.2c00090
JACS Au 2022, 2, 1811−1817

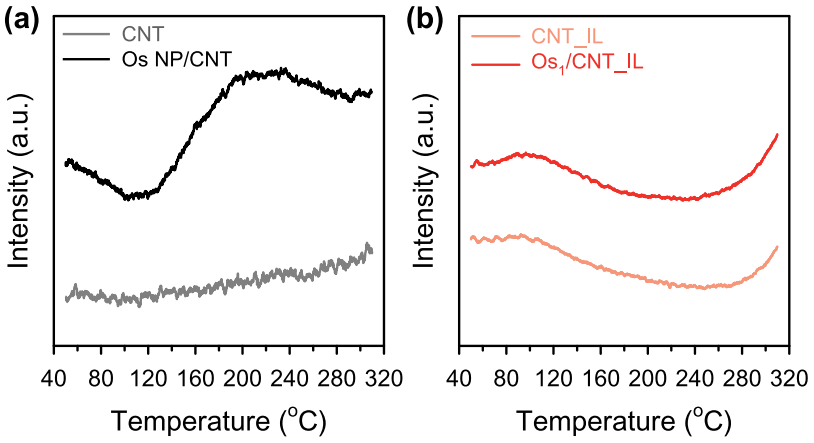

Figure 2. TPO profiles of (a) CNT and Os NP/CNT and (b) CNT_IL and Os_1/CNT_IL.

thermal stability of the atomically dispersed Os catalyst under air atmosphere compared with that of the unstable Os NP catalyst.

Next, we investigated the oxidation behaviors of the Os NP and atomically dispersed Os catalysts using TPO analyses. Prior to the TPO experiments, the samples were pretreated under a He flow at 400 °C to remove any physisorbed impurities. TPO was performed under a 50% O_2/He balance atmosphere at a ramping rate of 10 °C min^{-1}. The oxidation peak in the TPO profile of the Os NP/CNT (Figure 2a) emerged at ∼130 °C. No oxidation peak was observed in the TPO profile of the CNT support; therefore, the oxidation peak in the TPO profile of Os NP/CNT is ascribed to the oxidation of Os NPs. The HAADF-STEM image of the Os NP/CNT sample that underwent TPO revealed that Os NPs were no longer present in the sample (Figure S9a). This was caused by the oxidation of Os NPs into volatile OsO_4 during TPO. Conversely, the TPO profile of Os_1/CNT_IL was similar to that of the CNT_IL support, indicating that Os oxidation did not occur at the atomically dispersed Os sites embedded in the support. The HAADF-STEM image of the post-TPO Os_1/CNT_IL sample confirmed the presence of stable singly dispersed Os species in this sample (Figure S9b). To consolidate the origin of the oxidation peak from the TPO profile of Os NP/CNT, we tried to detect the sublimated OsO_4 from mass spectrometry by collecting the exhaust gas at the outlet of the reactor with a gas chromatography−mass spectrometry (GC−MS) system. Here, we used Os NP/CNT containing 50 wt % Os to increase the concentration of OsO_4 in the exhaust gas exceeding the detection limit. The exhaust gas was collected in a Tedlar gas sampling bag connected to the outlet of the quartz reactor at 300 °C, which is a higher temperature than the TPO oxidation peak position. The resulting mass spectrum clearly showed the presence of Os and Os oxide species in the exhaust gas (Figure S10), confirming the oxidation of Os.

To further confirm the superior stability of atomically dispersed Os species compared with that of Os NPs, we additionally prepared catalysts containing both Os NPs and single Os sites together. The ratio of Os NPs to single Os sites was controlled by changing the thermal activation temperature. The catalysts are denoted as Os/CNT_IL_*T*, where *T* is the thermal activation temperature. The HAADF-STEM images of the Os/CNT_IL_*T* catalysts revealed that the formation of Os NPs on CNT_IL started at 700 °C, and Os agglomeration intensified as the thermal activation temperature was increased up to 900 °C (Figure 3a−d). When the activation-temperature-controlled catalysts were subjected to calcination at 250 °C for 10 h, only atomically dispersed Os sites were observed in the corresponding HAADF-STEM images (Figure 3e−h), indicating the selective oxidation of Os NPs leaving behind atomically dispersed Os species.

The ICP-OES analysis corroborated the HAADF-STEM results (Table S2). The Os content of Os/CNT_IL_600, which comprised only atomically dispersed Os sites, changed only marginally after calcination (1.59 → 1.57 wt %). The Os content of Os/CNT_IL_700 decreased slightly after calcination (1.68 → 1.59 wt %), whereas those of Os/CNT_IL_800 and Os/CNT_IL_900 decreased considerably after calcination (1.88 → 0.90 wt % and 2.35 → 0.65 wt %, respectively). The TPO analysis results of the activation-temperature-controlled catalysts further confirmed the selective oxidation of Os NPs (Figure S11). The TPO profile of Os/CNT_IL_600, which comprised only single Os sites, was similar to that of the CNT_IL support (Figure 2b). A small oxidation peak at ∼230 °C was observed in the TPO profile of Os/CNT_IL_700, and a more distinct oxidation peak appeared in the TPO profile of Os/CNT_IL_900. The HAADF-STEM and TPO results demonstrated the unique thermal stability of atomically dispersed Os species, which was significantly higher than that of volatile Os NPs. We note that the peak temperature of Os/CNT_IL_900 is higher than that of Os NP/CNT by ∼40 °C, indicating that the Os NPs on bare CNTs are more vulnerable to the oxidation compared to those on CNT_IL. These results imply that the presence of nitrogen is effective to stabilize Os from oxidation, and the superior thermal stability of atomically dispersed Os catalysts may originate from the presence of Os−N bonds.

CO Oxidation Reaction

To evaluate the effect of the thermal stability of Os catalysts against oxidation to generate OsO_4, we selected CO oxidation under excess O_2 conditions as the model reaction (see the Materials and Methods section for the detailed reaction conditions). The light-off CO oxidation curves of Os NP/CNT, Os_1/CNT_IL, CNT, and CNT_IL in the temperature range of 50−450 °C are presented in Figure 4a. The supports (CNT and CNT_IL) exhibited no activity, regardless of heteroatom doping. The T_{50} (temperature at which 50% CO conversion was reached) value of Os NP/CNT (270 °C) was lower than that of Os_1/CNT_IL (330 °C), indicating the

https://doi.org/10.1021/jacsau.2c00090
JACS Au 2022, 2, 1811−1817

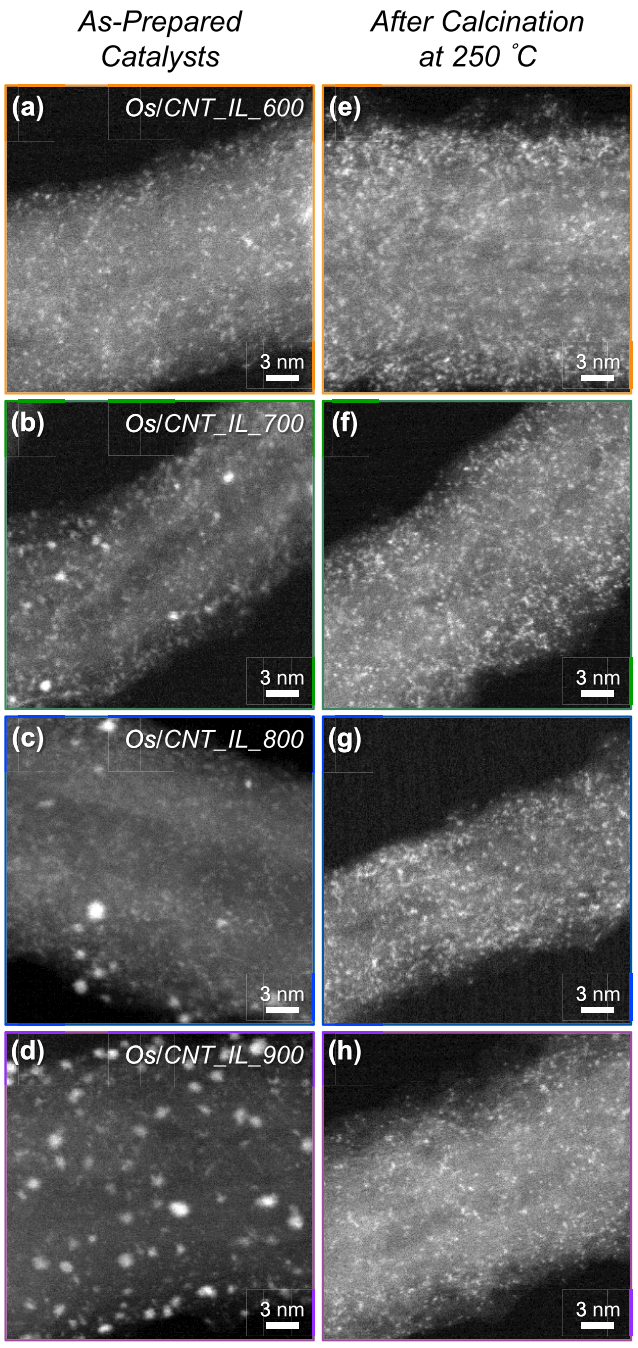

Figure 3. HAADF-STEM images of the (a) as-prepared and (e) calcined Os/CNT_IL_600, (b) as-prepared and (f) calcined Os/CNT_IL_700, (c) as-prepared and (g) calcined Os/CNT_IL_800, and (d) as-prepared and (h) calcined Os/CNT_IL_900. Calcination was performed at 250 °C.

better activity of Os NP/CNT. The corresponding activation energies of Os NP/CNT and Os_1/CNT_IL, which were calculated at conversions lower than 20% (kinetic regime), were 43.73 and 107.88 kJ/mol, respectively (Figure S12).

Although the initial CO oxidation activity of Os NP/CNT was higher than that of Os_1/CNT_IL, the former underwent a significant activity loss (86%) after 30 h of stability testing at 400 °C (Figure 4b). In stark contrast, the Os_1/CNT_IL preserved its initial CO oxidation activity (100%) over time. The HAADF-STEM image of Os NP/CNT after the stability test illustrated that most of Os NPs disappeared from the catalyst (Figure S13). The ICP results of Os NP/CNT showed that the content of Os became 0.02 wt % after a 30 h stability test (Table S3), supporting the HAADF-STEM result. This indicated that the deactivation of Os NP/CNT was caused by the formation of OsO_4 from Os NPs. In contrast, the single Os sites of Os_1/CNT_IL were preserved after 30 h of reaction. These results suggested the utility of atomically dispersed Os as a thermally stable, sustainable catalyst.

CONCLUSIONS

In summary, we demonstrated the remarkable thermal stability of atomically dispersed Os catalysts against an undesirable side reaction with O_2, which generates toxic and volatile OsO_4. The HAADF-STEM, ICP-OES, and TPO results revealed that Os NPs were oxidized into OsO_4, which subsequently sublimated at 130 °C. In contrast, atomically dispersed Os species were resistant to oxidation up to 300 °C. Owing to its remarkable thermal stability, the CO conversion of the atomically dispersed Os catalyst was stable (100%) over 30 h during the CO oxidation reaction; in contrast, the activity of the Os NP catalyst decreased considerably. We expect that our results would provide a new momentum to rejuvenate the potential of Os-based catalysts, which has been thus far hidden in the veil of their volatility and toxicity.

MATERIALS AND METHODS

Chemicals

Multiwalled CNTs (MR 99) were purchased from Carbon Nano-Material Technology Co., Ltd. HNO_3 (60%), HCl (36%), KOH (95%), methanol (99.9%), acetone (99.7%), ethanol (94.5%), and anhydrous ethanol (99.9%) were acquired from Samchun Chemicals. Dihydrogen hexachloroosmate(IV) hydrate ($H_2OsCl_6{\cdot}xH_2O$; Premion, 99.95%) and KNO_3 (99%) were obtained from Alfa Aesar. Tetraethyl orthosilicate (TEOS, 98%) and 1-butyl-3-methylimidazolium bis(trifluoromethylsulfonyl)imide (BMITFSI; 98%) ionic liquid (IL) were purchased from Aldrich. HF (50%) was supplied by J. T. Baker. Deionized (DI) water was produced using a Millipore Milli-Q system (18.2 MΩ). N_2 (99.999%), H_2 (99.999%), CO (5.00% balanced with Ar), O_2 (5.00% balanced with Ar), and Ar (99.999%) gases were procured from KOSEM. All the chemicals except for the CNTs were used as received without further purification.

Synthesis of Os NP/CNT

First, the metallic impurities in the CNTs were removed via successive heat and acid treatments. Next, 38 g of CNTs were heat-treated at 500 °C under air atmosphere for 1 h (ramping rate of 7.9 °C min^{-1}). The calcined CNTs were dispersed in 810 g of 6 M HNO_3 and stirred for 12 h at 80 °C. The dispersion was vacuum-filtered and washed with copious amounts of DI water until the filtrate became neutral. The resulting CNTs were treated with 720 g of 6 M HCl using the same procedure as for the HNO_3 treatment, followed by drying at 60 °C overnight to obtain acid-treated CNTs (AT-CNTs). $H_2OsCl_6{\cdot}xH_2O$ was loaded onto the AT-CNTs via wet impregnation as follows: 8 mg of $H_2OsCl_6{\cdot}xH_2O$ was dissolved in 20 g of methanol using a microwave (MARS 6, CEM corporation) at 600 W and 150 °C. The Os-precursor-dissolved methanol solution was mixed with 97 mg of AT-CNTs and dried at 40 °C under stirring. The Os-precursor-impregnated sample was reduced at 200 °C for 2 h (ramping rate of 0.58 °C min^{-1}) under a H_2 flow, followed by the desorption of H_2 from the Os surface via heating at 350 °C for 3 h (ramping rate of 2.5 °C min^{-1}) under a N_2 flow. The resulting sample is denoted as Os NP/CNT.

Synthesis of Os_1/CNT_IL and Os/CNT_IL_*T*

To generate abundant anchoring sites for the Os precursor on the support, AT-CNTs were coated with an IL. AT-CNTs (0.1 g) were mixed with BMITFSI (1.44 g) in a mortar for 15 min. The sticky

https://doi.org/10.1021/jacsau.2c00090
JACS Au 2022, 2, 1811−1817

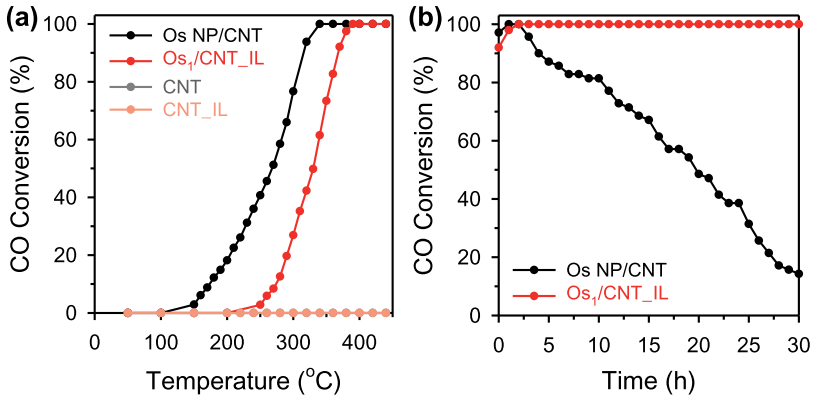

Figure 4. (a) Light-off CO oxidation curves of CNT, Os NP/CNT, CNT_IL, and Os_1/CNT_IL. (b) CO oxidation stability tests of Os NP/CNT and Os_1/CNT_IL at 400 °C.

mixture was pyrolyzed at 450 °C for 1 h (ramping rate of 5.3 °C min^{-1}) under a N_2 flow. The hardened product was ground in a mortar and washed with copious amounts of acetone via vacuum filtration to remove the IL physisorbed on the AT-CNTs. The resulting sample was dried at 60 °C overnight, and the product is denoted as CNT_IL. The Os precursor was impregnated onto the CNT_IL via microwave mixing using a methanol (20 g) solution of $H_2OsCl_6{\cdot}xH_2O$ (8 mg) and 97 mg of CNT_IL, and the mixture was dried at 40 °C under stirring. Next, the Os-impregnated CNT_IL was coated with a SiO_2 layer by mixing the former with 2.5 mL of TEOS in a mortar for 5 min. The mixture was dried overnight at room temperature (RT). The resulting sample was thermally activated at temperatures in the range of 500−900 °C for 3 h (ramping rate of 2.2 °C min^{-1}) under a N_2 flow. Thereafter, the SiO_2 layers were selectively etched via HF treatment. The catalyst activated at 500 °C is denoted as Os_1/CNT_IL, and the other catalysts are denoted as Os/CNT_IL_*T*, where *T* is the thermal activation temperature.

Characterization Methods

HAADF-STEM images were obtained using a JEOL-2100F microscope equipped with a double-sided spherical aberration corrector operated at an accelerating voltage of 200 kV. XPS spectra were taken using an instrument equipped with a monochromatic Al Kα radiation source (Thermo Fisher Scientific, ESCALAB 250XI). The N 1s XPS spectra were deconvoluted using the XPSPeak41 software with the mixed (Gaussian 70, Lorentzian 30) function after Shirley-type background correction. The Os contents of the catalysts were quantified using an ICP-OES analyzer (700-ES, Varian). For the pretreatment step of the ICP-OES experiments, 20 mg of the Os-containing sample was mixed with 1 g of KOH and 0.2 g of KNO_3. The mixed powder was transferred to an alumina crucible and annealed in a mini tube furnace by increasing the temperature from RT to 450 °C over 1 h (ramping rate of 2.2 °C min^{-1}) followed by maintaining the temperature at 450 °C for 1 h under a N_2 flow. After annealing, the sample was collected in a conical tube that contained 20 mL of H_2O. The GC−MS system (450-GC and 320-MS; Bruker) was equipped with a SCION-5MS (SCION Instruments) column (30 m × 0.25 mm × 0.25 μm). The sample gas (0.5 mL) was injected with the split-less mode using He as the carrier gas. The column was initially kept at 40 °C for 5 min and then ramped to 280 °C with a rate of 20 °C min^{-1}.

X-ray Absorption Spectroscopy (XAS)

XAS measurements were performed at the 6D, 8C, and 10C beamlines of the Pohang Accelerator Laboratory. The storage ring was operated at an energy of 3 GeV and a beam current of 400 mA. A Si(111) double-crystal monochromator was used to filter the incident photon energy, which was detuned by 30% for the Os L_3-edges to remove any high-order harmonics. The samples used for XAS measurements were pelletized in a sample holder. The Athena and Artemis software were used for background removal and normalization of the absorption coefficient and fitting of the Fourier transformed k^3-weighted EXAFS spectra, respectively.[39] The amplitude reduction factor (S_0^2) was set at 0.83.[40]

Temperature-Programmed Oxidation (TPO)

TPO profiles were obtained using a BELCAT II instrument (MicrotracBEL) equipped with a thermal conductivity detector (TCD). Prior to collecting the TPO profiles, 60 mg of each sample was degassed at 400 °C for 1 h (ramping rate of 10 °C min^{-1}) under a He flow to eliminate preadsorbed molecules. After cooling the samples, the TPO experiments were performed under a 50% O_2/He gas flow by heating each sample to 400 °C at a ramping rate of 10 °C min^{-1}.

CO Oxidation

CO oxidation was performed in a quartz fixed-bed reactor using 50 mg of the Os catalyst. The temperature was monitored using a thermocouple located inside the reactor. Prior to the measurements, each catalyst was pretreated at 100 °C under an Ar flow for 1 h. The CO oxidation reactions were performed using a feed stream of 2% CO and 4% O_2 balanced with Ar. The total flow rate and heating rate were 50 mL min^{-1} and 5 °C min^{-1}, respectively. The reaction mixture was maintained at each temperature for 10 min under a continuous feed flow to allow it to reach a steady state before each measurement. The obtained product was analyzed using a gas chromatograph (YL-6500) equipped with a Carboxen 1000 column (Supelco) and a TCD. The reaction rates (k) were calculated using the amount of CO_2 molecules produced per Os active site per second. The number of Os active sites was determined using the Os contents of the catalysts and ICP-OES experiments. The activation energy of each catalyst was determined from the corresponding Arrhenius plots, for which only the activity data with a CO conversion of less than 20% were considered (kinetic regime).

■ ASSOCIATED CONTENT

Supporting Information

The Supporting Information is available free of charge at https://pubs.acs.org/doi/10.1021/jacsau.2c00090.

Photographs of vial containing catalysts; particle size distribution; EXAFS fitting results; and XPS, XANES, HAADF-STEM, ICP-OES, and TPO, GC−MS and activation energy results (PDF)

■ AUTHOR INFORMATION

Corresponding Authors

Kwangjin An − *School of Energy and Chemical Engineering, Ulsan National Institute of Science and Technology (UNIST), Ulsan 44919, Republic of Korea;* orcid.org/0000-0002-5239-0296; Email: kjan@unist.ac.kr

https://doi.org/10.1021/jacsau.2c00090
JACS Au 2022, 2, 1811−1817

Sang Hoon Joo − *Department of Chemistry, Ulsan National Institute of Science and Technology (UNIST), Ulsan 44919, Republic of Korea;* orcid.org/0000-0002-8941-9662; Email: shjoo@unist.ac.kr

Authors

Jae Hyung Kim − *School of Energy and Chemical Engineering, Ulsan National Institute of Science and Technology (UNIST), Ulsan 44919, Republic of Korea; Clean Fuel Research Laboratory, Korea Institute of Energy Research, Daejeon 34129, Republic of Korea*

Sinmyung Yoon − *School of Energy and Chemical Engineering, Ulsan National Institute of Science and Technology (UNIST), Ulsan 44919, Republic of Korea;* orcid.org/0000-0003-2103-8772

Du San Baek − *Department of Chemistry, Ulsan National Institute of Science and Technology (UNIST), Ulsan 44919, Republic of Korea*

Jihun Kim − *School of Energy and Chemical Engineering, Ulsan National Institute of Science and Technology (UNIST), Ulsan 44919, Republic of Korea*

Jinjong Kim − *Department of Chemistry, Ulsan National Institute of Science and Technology (UNIST), Ulsan 44919, Republic of Korea*

Complete contact information is available at: https://pubs.acs.org/10.1021/jacsau.2c00090

Author Contributions

[‖]J.H.K., S.Y., and D.S.B. contributed equally to this work.

Notes

The authors declare no competing financial interest.

■ ACKNOWLEDGMENTS

This work was supported by the National Research Foundation (NRF) of Korea funded by the Ministry of Science and ICT (MSIT; NRF-2019M3E6A1064521, NRF-2019M3D1A1079306, NRF-2019M1A2A2065614, NRF-2020R1A5A1019631, NRF-2021R1A2C2006713, and NRF-2021R1A2C2007495). The X-ray absorption spectroscopy experiments performed at beamlines 6D, 8C, and 10C of the Pohang Accelerator Laboratory (PAL) were supported, in part, by the MSIT, Pohang University of Science of Technology (POSTECH), and UCRF at UNIST.

■ REFERENCES

(1) Jacobsen, E. N.; Markó, I.; Mungall, W. S.; Shröder, G.; Sharpless, K. B. Asymmetric Dihydroxylation via Ligand-Accelerated Catalysis. *J. Am. Chem. Soc.* **1988**, *110*, 1968−1970.

(2) Kolb, H. C.; Van Nieuwenhze, M. S.; Sharpless, K. B. Catalytic Asymmetric Dihydroxylation. *Chem. Rev.* **1994**, *94*, 2483−2546.

(3) Bond, G. C.; Webb, G. Ruthenium and Osmium as Hydrogenation Catalysts. *Platinum Met. Rev.* **1962**, *6*, 12−19.

(4) Chelucci, G.; Baldino, S.; Baratta, W. Recent Advances in Osmium-Catalyzed Hydrogenation and Dehydrogenation Reactions. *Acc. Chem. Res.* **2015**, *48*, 363−379.

(5) Bertoli, M.; Choualeb, A.; Lough, A. J.; Moore, B.; Spasyuk, D.; Gusev, D. G. Osmium and Ruthenium Catalysts for Dehydrogenation of Alcohols. *Organometallics* **2011**, *30*, 3479−3482.

(6) Tutton, A. E. The Chemistry of Osmium. *Nature* **1893**, *47*, 400−403.

(7) Occupational Safety and Health Administration. Permissible Exposure Limits − Annotated Tables. https://www.osha.gov/annotated-pels (accessed January 23, 2022).

(8) Nagayama, S.; Endo, M.; Kobayashi, S. Microencapsulated Osmium Tetraoxide. A New Recoverable and Reusable Polymer-Supported Osmium Catalyst for Dihydroxylation of Olefins. *J. Org. Chem.* **1998**, *63*, 6094−6095.

(9) Kobayashi, S.; Endo, M.; Nagayama, S. Catalytic Asymmetric Dihydroxylation of Olefins Using a Recoverable and Reusable Polymer-Supported Osmium Catalyst. *J. Am. Chem. Soc.* **1999**, *121*, 11229−11230.

(10) Choudary, B. M.; Chowdari, N. S.; Kantam, M. L.; Reghavan, K. V. Catalytic Asymmetric Dihydroxylation of Olefins with New Catalysts: The First Example of Heterogenization of OsO_4^{2-} by Ion-Exchange Technique. *J. Am. Chem. Soc.* **2001**, *123*, 9220−9221.

(11) Severeyns, A.; De Vos, D. E.; Fiermans, L.; Verpoort, F.; Grobet, P. J.; Jacobs, P. A. A Heterogeneous cis-Dihydroxylation Catalyst with Stable, Site-Isolated Osmium-Diolate Reaction Centers. *Angew. Chem., Int. Ed.* **2001**, *40*, 586−589.

(12) Choudary, B. M.; Chowdari, N. S.; Jyothi, K.; Kantam, M. L. Catalytic Asymmetric Dihydroxylation of Olefins with Reusable OsO_4^{2-} on Ion-Exchangers: The Scope and Reactivity Using Various Cooxidants. *J. Am. Chem. Soc.* **2002**, *124*, 5341−5349.

(13) Yao, Q. OsO_4 in Ionic Liquid $[Bmim]PF_6^-$ A Recyclable and Reusable Catalyst System for Olefin Dihydroxylation. Remarkable Effect of DMAP. *Org. Lett.* **2002**, *4*, 2197−2199.

(14) Lazarus, L. L.; Brutchey, R. L. Heterogeneous Fullerene-Supported Osmium Tetroxide Catalyst for the *cis*-Dihydroxylation of Olefins. *Dalton Trans.* **2010**, *39*, 7888−7890.

(15) Akiyama, R.; Matsuki, N.; Nomura, H.; Yoshida, H.; Yoshida, T.; Kobayashi, S. Nontoxic, Nonvolatile, and Highly Efficient Osmium Catalysts for Asymmetric Dihydroxylation of Alkenes and Application to One Mol-Scale Synthesis of an Anticancer Drug, Camptothecin Intermediate. *RSC Adv.* **2012**, *2*, 7456−7461.

(16) Metin, Ö.; Alp, N. A.; Akbayrak, S.; Biçer, A.; Gültekin, M. S.; Özkar, S.; Bozkaya, U. Dihydroxylation of Olefins Catalyzed by Zeolite-Confined Osmium(0) Nanoclusters: An Efficient and Reusable Method for the Preparation of 1,2-*cis*-Diols. *Green Chem.* **2012**, *14*, 1488−1492.

(17) Basavaraju, K. C.; Sharma, S.; Maurya, R. A.; Kim, D. P. Safe Use of a Toxic Compound: Heterogeneous OsO_4 Catalysis in a Nanobrush Polymer Microreactor. *Angew. Chem., Int. Ed.* **2013**, *52*, 6735−6738.

(18) Cano, R.; Pérez, J. M.; Ramón, D. J. Osmium Impregnated on Magnetite as a Heterogeneous Catalyst for the *syn*-Dihydroxylation of Alkenes. *Appl. Catal., A* **2014**, *470*, 177−182.

(19) Zhu, J.; Sun, X.-T.; Wang, X.-D.; Wu, L. Enantioselective Dihydroxylation of Alkenes Catalyzed by 1,4-Bis(9-*O*-dihydroquinidinyl)phthalazine-Modified Binaphthyl−Osmium Nanoparticles. *ChemCatChem* **2018**, *10*, 1788−1792.

(20) Fu, Q.; Saltsburg, H.; Flytzani-Stephanopoulos, M. Active Nonmetallic Au and Pt Species on Ceria-Based Water-Gas Shift Catalysts. *Science* **2003**, *301*, 935−938.

(21) Kwak, J. H.; Hu, J.; Mei, D.; Yi, C.-W.; Kim, D. H.; Peden, C. H. F.; Allard, L. F.; Szanyi, J. Coordinatively Unsaturated Al^{3+} Centers as Binding Sites for Active Catalyst Phases of Platinum on Gamma-Al_2O_3. *Science* **2009**, *325*, 1670−1673.

(22) Qiao, B.; Wang, A.; Yang, X.; Allard, L. F.; Jiang, Z.; Cui, Y.; Liu, J.; Li, J.; Zhang, T. Single-Atom Catalysis of CO Oxidation Using Pt_1/FeO_x. *Nat. Chem.* **2011**, *3*, 634−641.

(23) Cui, X.; Li, W.; Ryabchuk, P.; Junge, K.; Beller, M. Bridging Homogeneous and Heterogeneous Catalysis by Heterogeneous Single-Metal-Site Catalysts. *Nat. Catal.* **2018**, *1*, 385−397.

(24) Wang, A.; Li, J.; Zhang, T. Heterogeneous Single-Atom Catalysis. *Nat. Rev. Chem.* **2018**, *2*, 65−81.

(25) Mitchell, S.; Perez-Ramirez, J. Single Atom Catalysis: a Decade of Stunning Progress and the Promise for a Bright Future. *Nat. Commun.* **2020**, *11*, No. 4302.

(26) Ji, S.; Chen, Y.; Wang, X.; Zhang, Z.; Wang, D.; Li, Y. Chemical Synthesis of Single Atomic Site Catalysts. *Chem. Rev.* **2020**, *120*, 11900−11965.

(27) Speck, F. D.; Kim, J. H.; Bae, G.; Joo, S. H.; Mayrhofer, K. J. J.; Choi, C. H.; Cherevko, S. Single-Atom Catalysts: A Perspective toward Application in Electrochemical Energy Conversion. *JACS Au* **2021**, *1*, 1086−1100.
(28) Guo, X.; Fang, G.; Li, G.; Ma, H.; Fan, H.; Yu, L.; Ma, C.; Wu, X.; Deng, D.; Wei, M.; Tan, D.; Si, R.; Zhang, S.; Li, J.; Sun, L.; Tang, Z.; Pan, X.; Bao, X. Direct, Nonoxidative Conversion of Methane to Ethylene, Aromatics, and Hydrogen. *Science* **2014**, *344*, 616−619.
(29) Yang, S.; Kim, J.; Tak, Y. J.; Soon, A.; Lee, H. Single-Atom Catalyst of Platinum Supported on Titanium Nitride for Selective Electrochemical Reactions. *Angew. Chem., Int. Ed.* **2016**, *55*, 2058−2062.
(30) Lin, L.; Zhou, W.; Gao, R.; Yao, S.; Zhang, X.; Xu, W.; Zheng, S.; Jiang, Z.; Yu, Q.; Li, Y.-W.; Shi, C.; Wen, X.-D.; Ma, D. Low-Temperature Hydrogen Production from Water and Methanol Using Pt/α-MoC Catalysts. *Nature* **2017**, *544*, 80−83.
(31) Gu, J.; Hsu, C.-S.; Bai, L.; Chen, G. M.; Hu, X. Atomically Dispersed Fe^{3+} Sites Catalyze Efficient CO_2 Electroreduction to CO. *Science* **2019**, *364*, 1091−1094.
(32) Lim, T.; Jung, G. Y.; Kim, J. H.; Park, S. O.; Park, J.; Kim, Y.-T.; Kang, S. J.; Jeong, H. Y.; Kwak, S. K.; Joo, S. H. Atomically Dispersed Pt−N_4 Sites as Efficient and Selective Electrocatalysts for the Chlorine Evolution Reaction. *Nat. Commun.* **2020**, *11*, No. 412.
(33) Lim, T.; Kim, J. H.; Kim, J.; Baek, D. S.; Shin, T. J.; Jeong, H. Y.; Lee, K.-S.; Exner, K. S.; Joo, S. H. General Efficacy of Atomically Dispersed Pt Catalysts for the Chlorine Evolution Reaction: Potential-Dependent Switching of the Kinetics and Mechanism. *ACS Catal.* **2021**, *11*, 12232−12246.
(34) Kim, J. H.; Shin, D.; Kim, J.; Lim, J. S.; Paidi, V. K.; Shin, T. J.; Jeong, H. Y.; Lee, K.-S.; Kim, H.; Joo, S. H. Reversible Ligand Exchange in Atomically Dispersed Catalysts for Modulating the Activity and Selectivity of the Oxygen Reduction Reaction. *Angew. Chem., Int. Ed.* **2021**, *60*, 20528−20534.
(35) Kim, J. H.; Shin, D.; Lee, J.; Baek, D. S.; Shin, T. J.; Kim, Y.-T.; Jeong, H. Y.; Kwak, J. H.; Kim, H.; Joo, S. H. A General Strategy to Atomically Dispersed Precious Metal Catalysts for Unravelling Their Catalytic Trends for Oxygen Reduction Reaction. *ACS Nano* **2020**, *14*, 1990−2001.
(36) Qi, Z.; Xiao, C.; Liu, C.; Goh, T. W.; Zhou, L.; Maligal-Ganesh, R.; Pei, Y.; Li, X.; Curtiss, L. A.; Huang, W. Sub-4 nm PtZn Intermetallic Nanoparticles for Enhanced Mass and specific Activities in Catalytic Electrooxidation Reaction. *J. Am. Chem. Soc.* **2017**, *139*, 4762−4768.
(37) Sakakibara, N.; Takahashi, Y.; Okumura, K.; Hattori, K. H.; Yaita, T.; Suzuki, K.; Shimizu, H. Speciation of Osmium in an Iron Meteorite and a Platinum Ore Specimen Based on X-ray Absorption Fine-Structure Spectroscopy. *Geochem. J.* **2005**, *39*, 383−389.
(38) Takahashi, Y.; Uruga, T.; Suzuki, K.; Tanida, H.; Terada, Y.; Hattori, K. H. An Atomic Level Study of Rhenium and Radiogenic Osmium in Molybdenite. *Geochim. Cosmochim. Acta* **2007**, *71*, 5180−5190.
(39) Ravel, B.; Newville, M. ATHENAL, ARTEMIS, HEPHAESTUS: Data Analysis for X-ray Absorption Spectroscopy Using IFEFFIT. *J. Synchrotron Radiat.* **2005**, *12*, 537−541.
(40) Pitto-Barry, A.; Geraki, K.; Horbury, M. D.; Stavros, V. G.; Mosselmans, J. F. W.; Walton, R. I.; Sadler, P. J.; Barry, N. P. E. Controlled Fabrication of Osmium Nanocrystals by Electron, Laser and Microwave Irradiation and Characterisation by Microfocus X-ray Absorption Spectroscopy. *Chem. Commun.* **2017**, *53*, 12898−12901.

https://doi.org/10.1021/jacsau.2c00090
JACS Au 2022, 2, 1811−1817